Geophysical Research Letters

RESEARCH LETTER
10.1029/2024GL110598

Source Altitude of Energetic In-Cloud Pulses Inside Thunderstorms and Implication for the Intrinsic Brightness of Terrestrial Gamma-Ray Flashes

Fanchao Lyu[1,2], Zilong Qin[3], Steven A. Cummer[4], Yu Zheng[1], Sulin Jiang[1,2], Tianxue Zheng[1,2], Yan Liu[1], Wei Xu[5], and Weitao Lyu[1,2]

[1]Key Laboratory of Transportation Meteorology of China Meteorological Administration, Nanjing Joint Institute for Atmospheric Sciences, Nanjing, China, [2]State Key Laboratory of Severe Weather & CMA Key Laboratory of Lightning, Chinese Academy of Meteorological Sciences, Beijing, China, [3]Guangdong-Hong Kong-Macao Greater Bay Area Weather Research Center for Monitoring Warning and Forecasting (Shenzhen Institute of Meteorological Innovation), Shenzhen, China, [4]Electrical and Computer Engineering Department, Duke University, Durham, NC, USA, [5]Electronic Information School, Wuhan University, Wuhan, China

Abstract Upward Terrestrial Gamma-Ray Flashes (TGFs) are mainly produced during the upward propagating negative leaders inside thunderclouds. The exact source position of TGFs, which is crucial to understanding TGF source properties, is still unclear. The link between positive energetic in-cloud pulses (+EIPs) and TGFs provides us with a potential target to aim at. In this study, the low-frequency radio emissions of 75 +EIPs are analyzed to retrieve the source altitudes with an improved ray theory model. Furthermore, the meteorology contexts of +EIPs derived from the ground-based weather radars and satellite-based infrared cloud top temperature measurements are investigated. +EIPs are produced at 8.8–13.7 km, with an average of 11.3 km inside thunderclouds, and at an average of ∼2.5 km below cloud tops. These altitudes indicate that a total number of 1.7×10^{16} to 2.6×10^{18} gamma ray photons with energy greater than 1 MeV are required for an EIP-TGF to be measured by spaceborne detectors.

Plain Language Summary Terrestrial gamma-ray flashes (TGFs) are high-energy photon emissions generated during thunderstorms and related to the initial development of intra-cloud discharges. How TGFs are produced inside thunderclouds is still an open question, and one crucial issue is where TGFs are produced. Till now, it has been challenging to obtain the TGF positions directly. Recently, a distinct type of high-peak current events, which are named energetic in-cloud pulses (EIPs), are found to be closely linked to TGFs. The radio emissions of EIPs can be measured by ground-based radio sensors deployed hundreds of kilometers away from the source. In this study, a ray theory model is improved to retrieve the signature of very low-frequency/low-frequency radio signals of EIPs propagating in the Earth-ionosphere waveguide to obtain the source altitudes of EIPs. A total of 75 EIPs were found to be produced at 8.8–13.7 km, with an average of 11.3 km inside thunderclouds, and at an average of ∼2.5 km below cloud tops. With the source position information and combining the previously reported method to estimate the total number of source electrons, we suggest a total number of about 10^{17} is needed for TGFs being detected by spaceborne gamma ray detectors.

Key Points:

- An improved ray theory model is developed to retrieve energetic in-cloud pulse (EIP) positions
- Seventy-five +EIPs are located at 8.8–13.7 km, with a mean altitude of 11.3 km
- A mean gap of ∼2.5 km between EIPs and cloud tops was estimated

Supporting Information:

Supporting Information may be found in the online version of this article.

Correspondence to:

F. Lyu and S. A. Cummer,
lyufc@cma.gov.cn;
cummer@ee.duke.edu

Citation:

Lyu, F., Qin, Z., Cummer, S. A., Zheng, Y., Jiang, S., Zheng, T., et al. (2024). Source altitude of energetic in-cloud pulses inside thunderstorms and implication for the intrinsic brightness of terrestrial gamma-ray flashes. *Geophysical Research Letters*, *51*, e2024GL110598. https://doi.org/10.1029/2024GL110598

Received 12 JUN 2024
Accepted 31 AUG 2024

Author Contributions:

Conceptualization: Fanchao Lyu, Steven A. Cummer
Data curation: Fanchao Lyu, Sulin Jiang
Formal analysis: Fanchao Lyu, Zilong Qin
Funding acquisition: Fanchao Lyu
Investigation: Fanchao Lyu, Zilong Qin, Sulin Jiang, Tianxue Zheng, Yan Liu, Wei Xu
Methodology: Fanchao Lyu, Zilong Qin, Yu Zheng
Supervision: Steven A. Cummer, Weitao Lyu
Validation: Fanchao Lyu, Tianxue Zheng
Visualization: Yu Zheng, Sulin Jiang, Tianxue Zheng, Yan Liu, Wei Xu

1. Introduction

Terrestrial gamma-ray flashes (TGFs) are high-energy photon emissions that were generally observed by the gamma ray detector onboard satellites (Briggs et al., 2010; Fishman et al., 1994; Marisaldi et al., 2010; Østgaard et al., 2019; D. M. Smith et al., 2005). More and more observations on TGFs and their related lightning processes (Cohen et al., 2006; Connaughton et al., 2010; Cummer et al., 2011, 2014, 2015; Inan et al., 2006; Lu et al., 2010; Lyu et al., 2018; Mailyan et al., 2019; Pu et al., 2019; Shao et al., 2010; Stanley et al., 2006; Tilles et al., 2020; Xu et al., 2012; Zhang et al., 2020) generally confirmed that TGFs observed by satellite-based detectors were associated with the development of the initial stage of in-cloud discharges. They were produced during thunderclouds with either weak or deep convection cells (Chronis et al., 2016), and a wide range of cloud top temperatures (Ursi et al., 2019). It could be possible that some TGFs produced deep inside the thunderclouds were missed by the satellite-based gamma ray detectors, while only TGFs at higher altitudes were observed (D. M. Smith et al., 2010).

Writing – original draft: Fanchao Lyu, Zilong Qin
Writing – review & editing: Fanchao Lyu, Steven A. Cummer, Wei Xu, Weitao Lyu

The TGF source position is thus crucial to understanding the occurrence contexts and source properties of TGFs (Carlson et al., 2007; Dwyer et al., 2017; Hansen et al., 2013; Xu et al., 2015). Due to the challenges of source locating directly, coordinated observations from both the ground-based radio sensors and the satellite-based gamma ray detectors provided a potential method to understand where TGFs could be generated. Till now, only a few measurements on TGF source positions have been reported. They were first thought to be associated with the development of initial in-cloud leaders at 10–15 km (Lu et al., 2010; Shao et al., 2010; Stanley et al., 2006), but no detailed TGF source altitudes were determined because of the timing uncertainty. Cummer et al. (2015) measured the position and time of three TGF-associated upward propagating negative leaders and found that TGFs were produced at altitudes of 8–11 km during the middle position of the leaders. Pu et al. (2019) analyzed the simultaneity between a kind of slow pulses (Cummer et al., 2011; Dwyer & Cummer, 2013) and the gamma ray photon detected by Fermi-GBM. Based on the time alignment procedure between the slow pulse and the Fermi-observed TGF photons, the source positions were found ranging from 10 to 15 km for a total of six upward TGFs. Using a similar method, the source altitude of a downward TGF which produced the reverse positron seen by Fermi was determined to be at 7.5 ± 2.6 km (Chaffin et al., 2023). By combining the optical and gamma ray measurements from ASIM, Heumesser et al. (2021) estimated the positions of TGFs from the optical emissions of in-cloud leaders connected to the onset of TGFs, which placed TGFs at 1–5 km below the cloud tops.

While the detection of TGFs from space and determining the positions of TGFs is still challenging, the intrinsic link between a type of recently reported energetic in-cloud pulses (EIPs) and TGFs provides us a good candidate to investigate the possible source characteristics of some TGFs. EIPs are a distinct type of discharge produced during the development of negative leaders (Lyu & Cummer, 2018; Lyu et al., 2015). EIPs of positive polarity (+EIPs), which are produced during the upward negative leaders, are now known to be closely linked to a subset of TGFs (Lyu et al., 2016, 2021). Recent observations suggested that the low-frequency (LF) emission of +EIPs could be the direct current process of the relativistic discharges during the TGF process (Tilles et al., 2020). The close link between TGFs and +EIPs thus provides a useful approach to analyzing the source properties of TGF-producing processes. The altitudes of two TGFs associated with EIP-like processes were first investigated by Cummer et al. (2014), and a source altitude of around 12 km was found.

In this study, the statistical relationship between the +EIP source positions relative to the development of the thunderclouds was investigated, based on the comprehensive analysis of (a) the +EIPs and locations from the national lightning detection network (NLDN), (b) the source altitudes of +EIPs retrieved from an improved ray theory model, and (c) the properties of thundercloud tops retrieved from both the ground-based weather radars and satellite-based IR images. For a total of 75 events located in proper ranges of the LF sensors and ground-based weather radars, they were found to be produced at 8.8–13.7 km with a mean of 11.3 km, which placed the +EIPs at 0.1–6.3 km (with an average of ∼2.5 km) below the echo top of the thunderclouds. The high-energy electrons that are needed for an EIP-TGF to be observed were also estimated.

2. Method and Data Set

2.1. An Improved Ray Theory Model for Elevated Source Altitude Estimation

The VLF/LF sferics produced by an elevated source can propagate in the Earth-Ionosphere waveguide and be reflected by the boundary of the waveguide. In previous studies, the propagation geometry of the groundwave and skywaves has been directly used to calculate the source heights of IC events (Cummer et al., 2015; Lü et al., 2013; Lyu et al., 2015; D. A. Smith et al., 1999, 2004; Wu et al., 2012; Zhang et al., 2016). In recent studies, Qin et al. (2017, 2019) proposed a ray theory model to retrieve the propagation of VLF/LF signals in the Earth-ionosphere waveguide from a ground source, like return strokes from cloud-to-ground flashes (CGs). The waveform-based curve-fitting technique has been used to retrieve the electron density profile of the lower ionosphere (Han & Cummer, 2010; Qin et al., 2019; Shao et al., 2013) for a ground source. The electron density profiles, that is, reference height and sharpness (h', β, with h' in km and β in km^{-1}) in Wait's profile equation (Wait & Spies, 1964) are retrieved. Here we improved the ray theory model and applied it to an elevated source. The paths of the groundwave and skywave pairs from the source to the receiver are illustrated in Figure 1a. The skywave pairs are simulated and are used to estimate the altitudes of elevated sources.

Compared to the previously proposed ray theory model by Qin et al. (2019), in addition to the electron density profile, one more parameter, the source height h_s, was introduced in the improved ray theory model for elevated sources (See Supporting Information S1 for more information). Similarly, a curve-fitting between the simulations

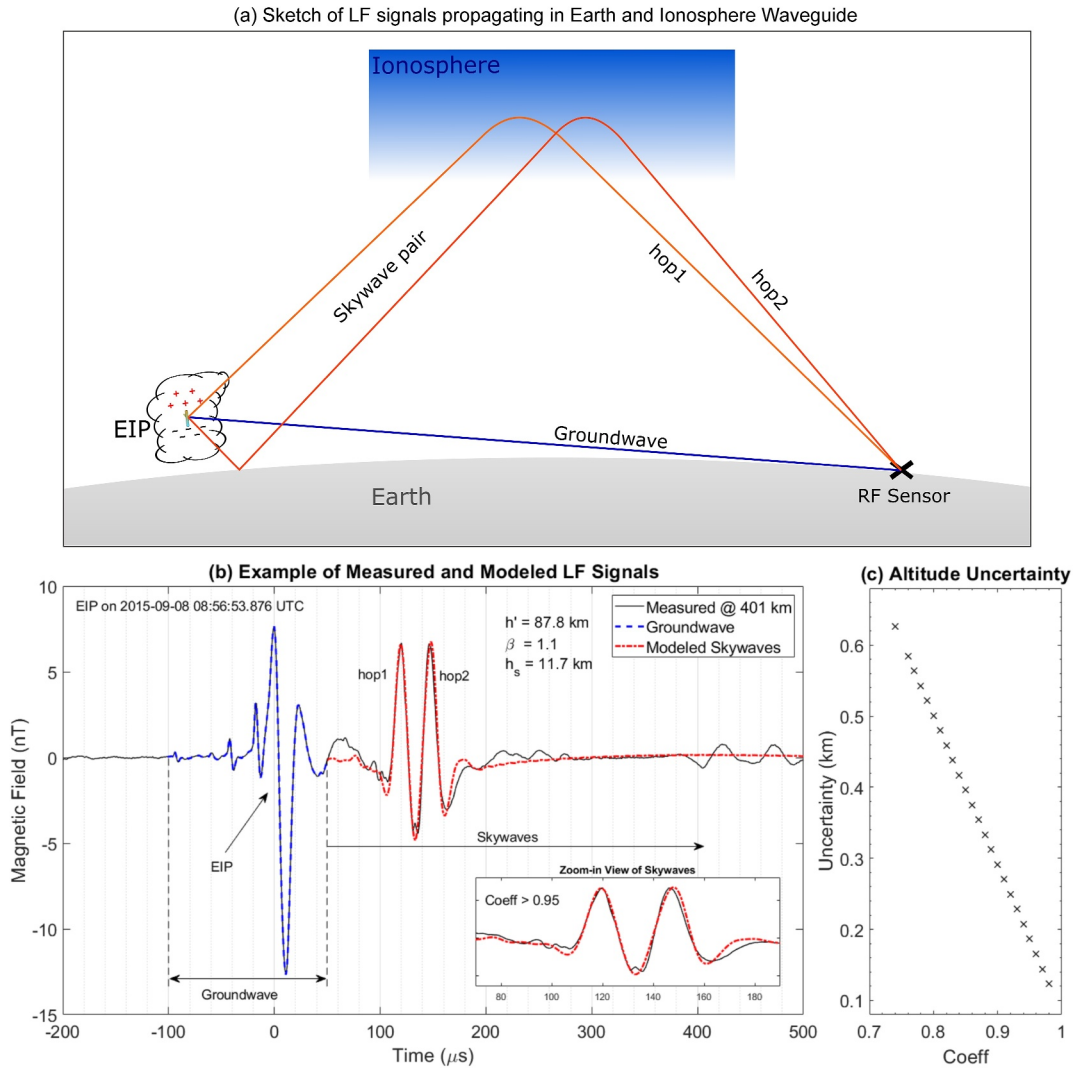

Figure 1. The method applied in this study. (a) Example of the measured low-frequency (LF) waveform of the groundwave and skywaves of an +EIP. (b) A source height of 11.7 km, ionospheric height of 87.8 km, and β of 1.1 km^{-1} was retrieved. The black line shows the measured LF waveform at the Florida Institute of Technology sensor, which is 401 km from the national lightning detection network location of the +EIP. The blue dashed waveform in the 250-μs window illustrates the groundwave signal, which serves as the input of our improved ray theory model. The red dashed waveform shows the modeled waveform of the skywave when a maximum cross coefficient of 0.959 is achieved. The zoom-in view of the skywaves is shown in the embedded panel in (b). (c) The altitude uncertainty which related to the cross-correlation coefficient between the measured and modeled LF signals.

and observations was applied, which allows us to find the best estimation for the parameters of a particular source. Possible ranges of different parameters were arbitrarily determined preceding the curve-fitting process based on previously reported results. TGFs, as well as EIPs, were reported to be produced in thunderclouds with source regions below around 20 km (Cummer et al., 2015; Dwyer & Smith, 2005; Lyu et al., 2015; Tilles et al., 2020). For simplicity, here we set the possible range of h_s from 0 to 20 km with an increasing step of 0.1 km, h' being from 70 to 90 km with a step of 0.1 km, β from 0.2 km^{-1} to 1.1 km^{-1} with a step of 0.1 km^{-1}. The Earth's magnetic field parameters were set to the local values of the +EIPs distribution region according to the World Magnetic Model (Chulliat et al., 2020). The calculation process was finally convergent to the result with the maximum correlation coefficient between the measured skywaves and modeled results, with h_s being the optimal source height of an +EIP. The height error could be reflected by the correlation coefficient. With a similar method in Cummer et al. (2014), an altitude uncertainty of ±(0.1–0.6) km for a cross-correlation coefficient of 0.98–0.74 was estimated for all the EIPs analyzed here (Figure 1c).

Figure 1b illustrates an example of the comparison between the measured and modeled LF signals of an +EIP. The main +EIP pulse in a 250-μs window was selected as the input of the groundwave of the ray theory model. Then the output of the model, which includes the time sequence of skywave pairs was compared with the measurements. As shown in Figure 1b, for the ionosphere parameters, h' and β being 87.8 km and 1.1 km^{-1}, the best cross-correlation coefficient of 0.959 between the modeled and measured skywaves was achieved. The source altitude of +EIP is found at 11.7 km.

2.2. LF Measurements, Radar Observations, and EIP Data Set

The measured waveform is crucial for the source altitude retrieval. The LF waveforms were measured by two ground-based LF sensors deployed at Duke Forest near Duke University and the Florida Institute of Technology (FIT). +EIPs analyzed were selected from the 1,334 EIPs reported by Lyu et al. (2021), with the following restricted conditions:

1. Because of the variation of the signal-to-noise ratio and the propagation effect of the radio frequency signals along the Earth-ionosphere waveguide, the measured waveform could be complicated. EIPs must be located within the proper range (not too close and too far) of each of the LF sensors, since both the ground wave and sky waves should be distinguished and modeled. Only those events that occurred within 400–700 km from Duke or FIT LF sensors were selected. Four events were recorded by both Duke and FIT sensors. From the modeled results, a source height discrepancy of ∼1 km can be obtained for the same event because of different waveform signatures recorded by two sensors. Thus, the LF waveform from one of the sensors showing more decent ground and skywaves was preferred.
2. EIPs should also be located within the detection range of one of the NEXRAD weather radars. Accordingly, a total of 75 EIPs were included in this study. For the +EIPs close enough to NEXRAD radars, the vertical profile along the lines crossing the ground location of +EIPs was analyzed to estimate the echo top of the cells. Both the raw data of the radar scans and the interpolated data were investigated, while the maximum height of 18 dBZ radar echo from the interpolated radar data was compared with EIP source height and the IR cloud top temperatures.

2.3. Merged-IR Cloud Top Temperature

The Merged-IR temperature product was used to retrieve the cloud top temperature of the thunderclouds. The merged-IR data contain globally merged (60°S–60°N) infra-red (IR) brightness temperature data from geostationary satellites with a pixel resolution of 4 km every half hour (Janowiak et al., 2017). Although the large time resolution of the IR images was not matched with the time of +EIPs (with a largest time interval of 15 min), the Merged-IR temperature product provided useful information on the EIP-producing cells. To retrieve the height of the IR cloud tops, the local atmospheric sounding data from the nearest station of the Wyoming Atmospheric Sounding and the lowest IR brightness temperatures in an approximate 15 km by 15 km region over the EIP positions was used. Note that the satellite-based IR brightness temperature and ground-based radar reflectivity are two distinct ways to retrieve the cloud tops. There could be a discrepancy in the cloud top heights inferred from the two different measurements, which, however in general, agree with each other within about 1 km (Castro et al., 2020; Naud et al., 2005).

3. Examples of +EIP Altitudes and the Meteorology Contexts of EIP-Producing Cells

Four +EIPs are presented here for a detailed illustration of +EIP positions and their meteorology contexts. Two +EIPs were produced during the passes of Fermi and were identified to be true TGFs (Briggs et al., 2010; Lyu et al., 2021; Roberts et al., 2018). Another two +EIPs were produced during different stages of a convective system, but no gamma ray measurements were available for them.

3.1. Two EIP-TGFs

Two +EIPs (EIP-TGF-1, EIP-TGF-2, hereinafter) were observed by Fermi-GBM (Briggs et al., 2010; Roberts et al., 2018). EIP-TGF-1 was directly reported by Fermi to be a TGF, while EIP-TGF-2 was originally missed by Fermi's general TGF identification criteria but was later identified from the search of +EIPs (Lyu et al., 2021). Detailed gamma ray signatures from Fermi-GBM and the observations from ground-based radio sensors of the two events can be found in Lyu et al. (2016, 2021). Figure 2 shows the IR cloud top temperature, the atmospheric

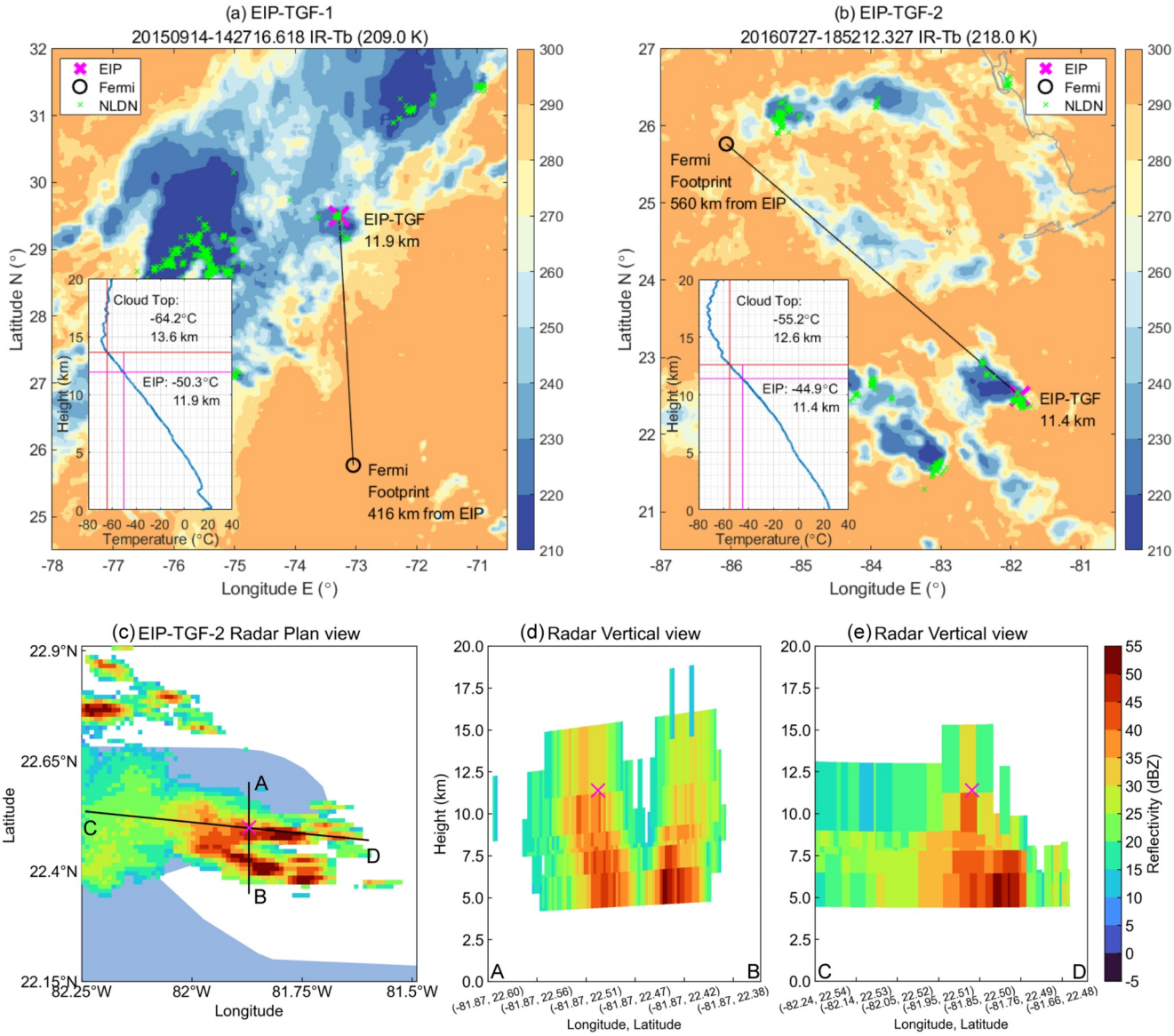

Figure 2. The IR cloud top temperature, the atmospheric sounding profile, and the NEXRAD radar scans (composite reflectivity) of the Energetic In-cloud Pulse (EIP)-producing storms. The black circle marks the position of the Fermi nadir. The magenta cross marks the national lightning detection network (NLDN) location of the +EIP. The green crosses in (a) and (b) illustrate the NLDN locations of lightning events within 5 min ([−5 5] mins) of EIP's occurrence. The atmospheric sounding profiles from the nearest sounding station are shown in the embedded figures. The temperature and height of cloud top and EIP position are marked by the vertical and horizontal lines of red and magenta, respectively. Panels (c–e) show the plan and vertical views of the radar scans of the cell producing EIP-TGF-2 observed by NEXRAD radar at KBYX, Key West at 18:51 UTC on 27 July 2016.

sounding profiles, and the radar observations of the EIP-producing storms from the measuring sites close to the storms. EIP-TGF-1 was produced in a small convective cell, which was embedded in the edge of a large developing mesoscale convection system. Two large convection cells with lower cloud top temperatures and more NLDN-reported lightning events can be found in the west and northeast regions of the large convection system. However, no EIPs were produced in those cells. From the combination of nearby atmospheric sounding and IR temperature, an IR cloud top of 13.6 km (−64.2°C) was estimated for the small EIP-producing cell. The EIP was estimated at 11.9 km, corresponding to a sounding temperature of −50.3°C at EIP's altitude, with a vertical gap of 1.7 km between the EIP source and the IR cloud top. EIP-TGF-1 was too far from ground-based weather radars.

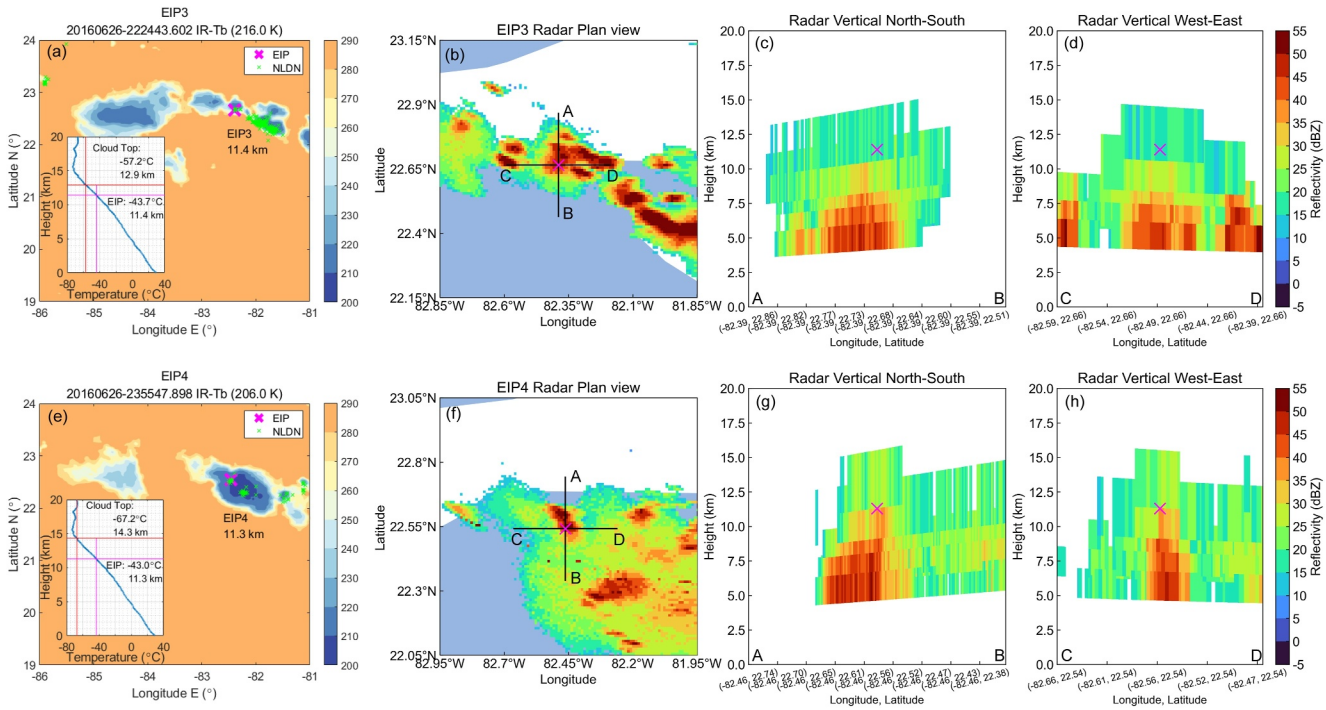

Figure 3. The cloud top temperature and the plan and vertical views of the radar echo (from KBYX radar, at Key West) of a storm producing two +EIPs in a 90-min time window. The color maps and the markers in each panel have the same means as those shown in Figure 2.

Comparatively, EIP-TGF-2 in Figure 2b was produced in a scattered thunderstorm system. Lightning events were detected in several cells with IR cloud top temperatures less than −40°C. EIP-TGF-2 was produced in the cell with the lowest cloud top temperature of −55.2°C, corresponding to an IR cloud top height of 12.6 km. EIP-TGF-2 was produced at 11.4 km, suggesting a sounding temperature of −44.9°C. Thus, a vertical gap of 1.2 km between the EIP source and the cloud top was obtained. This cell was close enough to the KBYX (Key West) NEXRAD weather radar. As illustrated in the plan view and vertical profiles of the raw data of radar scans in Figures 2c–2e, EIP-TGF-2 was produced at the edge of the 40-dBZ core, and in the upper region of the convective cell. The raw data of the radar scan indicated an upper limit of 3.5 km above the EIP position. The interpolated radar scans suggest an 18-dBZ top at 13.7 km, thus a gap of 2.3 km between the radar echo top and EIP-TGF-2.

Considering the modest time resolution of the IR cloud top temperature and the moderate space resolution of the radar scans at large distances, the vertical gaps between the two EIP-TGF sources and tops of the IR cloud and radar echo are comparable and reasonably consistent with the two cases reported by Cummer et al. (2014).

3.2. Two +EIPs Produced During Different Stages of One Convection System

Note that, because of the limited time window of a single satellite pass, it might be challenging for satellite-based detectors to observe multiple TGFs during one storm. Here we show the characteristics of two +EIPs, specifically EIP3 and EIP4, which were recorded during the development of one convection system. The scattered thunderclouds moved to the southeast slowly, with EIP4 being detected approximately 1.5 hr after EIP3. During this 1.5 hr, both the merging and splitting processes of different cells were observed by the ground-based weather radar, which suggests that EIP3 originated during the development stage, while EIP4 was produced during the dissipation stage.

The scattered thunderstorm contained multiple small areas with IR cloud tops below −40°C. EIP3 was produced at 11.4 km, indicating a sounding temperature of −43.7°C. It was in a region marked by the lowest cloud top temperature of −57.2°C, corresponding to an IR cloud top height of 12.9 km as shown in the embedded profile in Figure 3a. Although the radar echo image in Figure 3b reveals several regions with reflectivity above 50 dBZ, lightning events within the 5 min of the EIP were only detected in the EIP-producing cell and the larger one to the southeast. From the vertical profiles of the radar reflectivity shown in Figures 3c and 3d, EIP3 positioned above

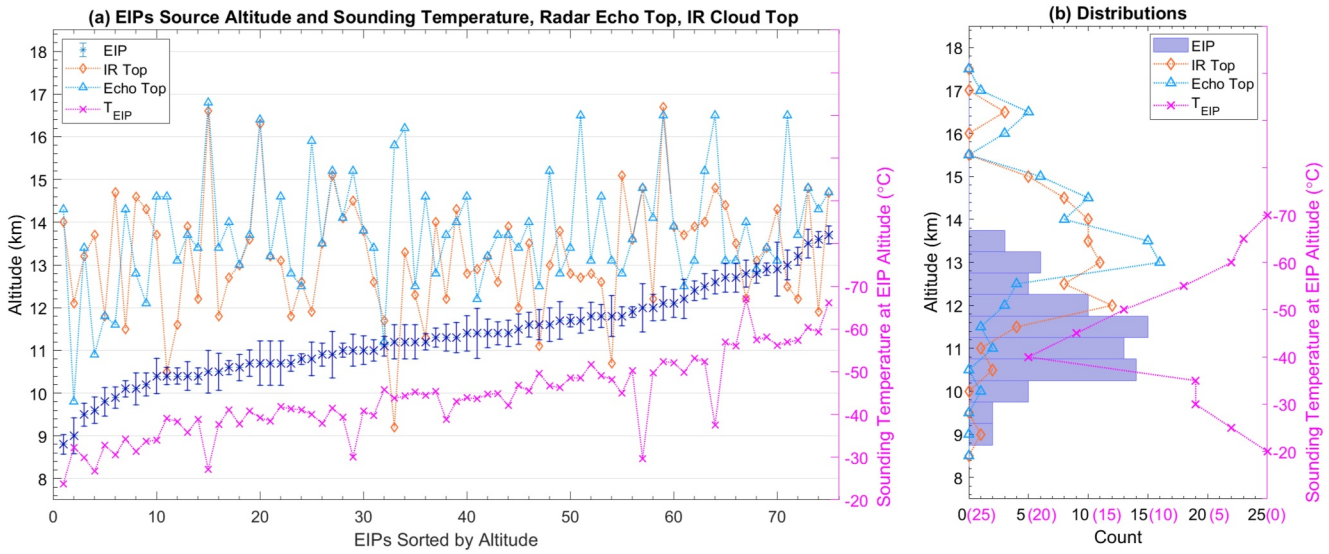

Figure 4. (a) The source altitudes of Energetic In-cloud Pulses (EIPs) and the cloud tops estimated from two different observations, EIPs are ordered by their altitudes. The source altitudes are shown by the blue crosses, with the altitude uncertainty marked by the error bars. The blue triangle-line shows the echo tops by ground-based radar, the orange diamond-line shows the cloud tops by the satellite-based IR measurements, and the magenta cross-line illustrates the temperature at EIP altitude from the sounding profile. (b) The distributions of EIP source altitudes, radar echo tops, the IR cloud tops, and the sounding temperature at EIP altitudes.

the 30-dBZ core region. The raw radar scan data demonstrated an upper limit of 13.7 km of the echo boundary. While the interpolated radar scans indicated an 18-dBZ top at 12.2 km, which is 0.8 km above the EIP.

The lowest cloud temperature close to EIP4's position was −67.2°C, indicating an IR cloud top height of 14.3 km. EIP4 was estimated at 11.3 km, indicating a sounding temperature of −43.0°C, which was 3.0 km beneath the IR cloud top. The composite radar reflectivity in Figure 3f displays fewer convection cells compared to those in Figure 3b, the IR image suggests a significantly larger area with a cloud top temperature lower than −40°C. EIP4 was generated during the storm's dissipation stage, characterized by fewer convective cells and lightning events, yet retaining an anvil due to the preceding intense convective activity. The radar's vertical profiles show that EIP4 appeared at the upper region of the 40-dBZ core, similar to EIP-TGF-2. An upper threshold of 3.7 km above the EIP4's position is yielded from the raw radar data, while the interpolated radar data suggests a gap of 2.6 km relative to the 18-dBZ top.

Both EIPs were produced at similar positions, which is also consistent with the two EIP-TGFs in Figure 2. Nonetheless, because of the different originated storm environments, gaps between different +EIPs and the cloud tops of their originated storms were distinct. EIP3 was estimated to be about 1.5 km below the cloud top, while EIP4 was produced at about 3 km beneath the cloud top. The variation in vertical separation between +EIPs and the cloud tops likely could result from variations in the developmental stages of storms.

4. Statistics of +EIP Source Altitudes and Its Implications

Figure 4 shows the statistics of the EIP source altitudes, the altitudes of the radar echo tops illustrated by the 18 dBZ radar reflectivity, the cloud tops retrieved from the IR cloud top temperature, and the sounding temperature at source altitudes for the 75 EIPs. +EIPs were generated between 8.8 and 13.7 km, with a mean value of 11.3 km, which is well consistent with the +EIP observed by the VHF interferometer (Tilles et al., 2020) and two EIP-TGF cases (Cummer et al., 2014). Nearly 70% of +EIPs were located in the range of 10–12 km. A standard deviation of ∼1.0 km was obtained, suggesting the moderate variation of EIPs' position in different storm environments. All +EIPs were produced at levels with sounding temperature between −20 and −70°C (mean of −43.9°C). Nearly 90% were located in regions with environment temperature between −30 and −55°C. The radar echo tops of the EIP-producing storms were estimated to be 9.8–16.2 km, with a mean value of 13.8 km. For the IR cloud tops, a few outliers showed their altitudes apparently lower than that of EIPs, which probably was because of the considerable time resolutions and uncertainty of the Merged-IR data. After removing those outliers, the cloud tops were between 10.5 and 16.7 km, with the mean of 13.4 km. Note that both radar echo top and IR cloud tops

retrieved here were somewhat higher but reasonably consistent with the enhanced echo tops of TGF-producing storms reported by Chronis et al. (2016). Combined with the temporal occurrence contexts of the +EIP sferics (Lyu et al., 2015, 2018), we suggest that there could be little chance for a +EIP to be produced above the thundercloud tops. In general, +EIPs are produced in thunderclouds with source altitudes lower than the cloud tops, with a mean vertical gap of 2.2–2.5 km between the +EIP positions and the cloud tops.

In view of the close link between +EIPs and upward TGFs (Lyu et al., 2016, 2021), the source parameters of EIPs are thus significant to understanding the source parameters of TGFs. The total number of source electrons can be determined by finding out the value that can explain the TGF fluence measured by satellites, specifically using a Monte Carlo model, similar to the method described by Mailyan et al. (2019), Xu et al. (2015) and Celestin et al. (2015). For EIPs produced between 13.7 and 8.8 km, we can estimate a possible range of 2.0×10^{16} to 3.0×10^{18}, and a mean value of 8.0×10^{16} electrons with energy greater than 10 keV being required for a standard detectable TGF. Considering the electrons with energy greater than 1 MeV, a total number of 1.7×10^{16} to 2.6×10^{18} with a mean value of 6.9×10^{16} is needed for TGFs being detected by spaceborne gamma ray detectors. For an upward EIP-TGF occurring at 8.8 km, which is the lower limit in this study, at least 2.6×10^{18} electrons are required for it to be detected by space-borne detectors.

5. Summary

In this study, the ray theory model developed for the propagation of VLF/LF signals on the ground was improved to simulate and retrieve the parameters of the elevated sources. The source altitudes of 75 +EIPs were investigated in detail. They were produced at altitudes ranging between 8.8 and 13.7 km (mean of 11.3 km), with 90% of them located in regions corresponding sounding temperatures between −30°C and −55°C (mean of −43.9°C). This could be a region above the main negative charge center and near the center of the upper positive charge region in thunderstorms. Combined with the cloud top heights retrieved from ground-based weather radars and IR cloud top temperatures, +EIPs were generated ∼2.5 km below the cloud tops. No +EIPs were found above 14 km. However, six +EIPs (8%) were produced deep inside the thunderclouds, with source altitudes lower than 10 km.

For the TGFs that are produced deep inside the thunderclouds, longer paths will be needed for the gamma ray photons propagating in the atmosphere with high density. Distinct light curves and spectrums of the high-energy emissions can be expected at the satellite-based instruments. Thus, at least two consequences can be expected for these TGFs: (a) For the TGF detection by gamma ray detectors onboard satellites, fewer gamma ray photons with energy above the identification threshold would be counted, which could lead to the omission of some of these TGFs. (b) For source property investigation using the gamma ray spectrum observed by detectors onboard satellites, the intrinsic brightness could be underestimated if the gamma ray sources were from much deeper positions inside the thunderclouds. In such circumstances (lower source altitudes and longer paths for electrons passing through high-density atmosphere), for the TGFs that would be seen by the satellite-based detectors, like Fermi-GBM or ASIM, a larger number of total electrons would be required.

Data Availability Statement

This study complies with the AGU data policy. The measured and modeled lightning data used in this study is available at Lyu (2024). The KRAX radar data is available at https://www.ncdc.noaa.gov/nexradinv/map.jsp. The merged infrared brightness temperature data is available at Janowiak et al. (2017). The atmospheric sounding data is available at https://weather.uwyo.edu/upperair/sounding.html.

Acknowledgments
This work was supported in part by the Basic Research Fund of the Chinese Academy of Meteorological Sciences (Grants 2024Z010, 2020R004), and the National Natural Science Foundation of China (Grant 42104161). We thank two anonymous reviewers for their constructive comments and suggestions.

References

Briggs, M. S., Fishman, G. J., Connaughton, V., Bhat, P. N., Paciesas, W. S., Preece, R. D., et al. (2010). First results on terrestrial gamma ray flashes from the Fermi Gamma-ray Burst Monitor. *Journal of Geophysical Research*, *115*(A7), A07323. https://doi.org/10.1029/2009JA015242

Carlson, B. E., Lehtinen, N. G., & Inan, U. S. (2007). Constraints on terrestrial gamma ray flash production from satellite observation. *Geophysical Research Letters*, *34*(8), L08809. https://doi.org/10.1029/2006gl029229

Castro, E., Ishida, T., Takahashi, Y., Kubota, H., Perez, G. J., & Marciano, J. S. (2020). Determination of cloud-top height through three-dimensional cloud reconstruction using DIWATA-1 data. *Scientific Reports*, *10*(1), 7570. https://doi.org/10.1038/s41598-020-64274-z

Celestin, S., Xu, W., & Pasko, V. P. (2015). Variability in fluence and spectrum of high-energy photon bursts produced by lightning leaders. *Journal of Geophysical Research: Space Physics*, *120*(12), 10712–10723. https://doi.org/10.1002/2015ja021410

Chaffin, J. M., Pu, Y., Smith, D. M., Cummer, S., & Splitt, M. (2023). Determining a lower limit of luminosity for the first satellite observation of a reverse beam terrestrial gamma-ray flash associated with a cloud to ground lightning leader. *Journal of Geophysical Research: Atmospheres*, *128*(18), e2023JD038885. https://doi.org/10.1029/2023JD038885

Chronis, T., Briggs, M. S., Priftis, G., Connaughton, V., Brundell, J., Holzworth, R., et al. (2016). Characteristics of thunderstorms that produce terrestrial gamma ray flashes. *Bulletin of the American Meteorological Society*, *97*(4), 639–653. https://doi.org/10.1175/BAMS-D-14-00239.1

Chulliat, A., Brown, W., Alken, P., Beggan, C., Nair, M., Cox, G., et al. (2020). *The US/UK World Magnetic Model for 2020-2025: Technical Report*. National Centers for Environmental Information, NOAA. https://doi.org/10.25923/ytk1-yx35

Cohen, M. B., Inan, U. S., & Fishman, G. (2006). Terrestrial gamma ray flashes observed aboard the Compton Gamma Ray Observatory/Burst and Transient Source Experiment and ELF/VLF radio atmospherics. *Journal of Geophysical Research*, *111*(D24), D24109. https://doi.org/10.1029/2005JD006987

Connaughton, V., Briggs, M. S., Holzworth, R. H., Hutchins, M. L., Fishman, G. J., Wilson-Hodge, C. A., et al. (2010). Associations between Fermi Gamma-ray Burst Monitor terrestrial gamma ray flashes and sferics from the World Wide Lightning Location Network. *Journal of Geophysical Research*, *115*(A12), A12307. https://doi.org/10.1029/2010JA015681

Cummer, S. A., Briggs, M. S., Dwyer, J. R., Xiong, S. L., Connaughton, V., Fishman, G. J., et al. (2014). The source altitude, electric current, and intrinsic brightness of terrestrial gamma ray flashes. *Geophysical Research Letters*, *41*(23), 8586–8593. https://doi.org/10.1002/2014GL062196

Cummer, S. A., Lu, G. P., Briggs, M. S., Connaughton, V., Xiong, S. L., Fishman, G. J., & Dwyer, J. R. (2011). The lightning-TGF relationship on microsecond timescales. *Geophysical Research Letters*, *38*(14), L14810. https://doi.org/10.1029/2011GL048099

Cummer, S. A., Lyu, F., Briggs, M. S., Fitzpatrick, G., Roberts, O. J., & Dwyer, J. R. (2015). Lightning leader altitude progression in terrestrial gamma-ray flashes. *Geophysical Research Letters*, *42*(18), 7792–7798. https://doi.org/10.1002/2015GL065228

Dwyer, J. R., & Cummer, S. A. (2013). Radio emissions from terrestrial gamma-ray flashes. *Journal of Geophysical Research: Space Physics*, *118*(6), 3769–3790. https://doi.org/10.1002/jgra.50188

Dwyer, J. R., Liu, N. Y., Grove, J. E., Rassoul, H., & Smith, D. M. (2017). Characterizing the source properties of terrestrial gamma ray flashes. *Journal of Geophysical Research-Space Physics*, *122*(8), 8915–8932. https://doi.org/10.1002/2017JA024141

Dwyer, J. R., & Smith, D. M. (2005). A comparison between Monte Carlo simulations of runaway breakdown and terrestrial gamma-ray flash observations. *Geophysical Research Letters*, *32*(22), L22804. https://doi.org/10.1029/2005gl023848

Fishman, G. J., Bhat, P. N., Mallozzi, R., Horack, J. M., Koshut, T., Kouveliotou, C., et al. (1994). Discovery of intense gamma-ray flashes of atmospheric origin. *Science*, *264*(5163), 1313–1316. https://doi.org/10.1126/science.264.5163.1313

Han, F., & Cummer, S. A. (2010). Midlatitude daytime D region ionosphere variations measured from radio atmospherics. *Journal of Geophysical Research*, *115*(A10), A10314. https://doi.org/10.1029/2010ja015715

Hansen, R. S., Østgaard, N., Gjesteland, T., & Carlson, B. (2013). How simulated fluence of photons from terrestrial gamma ray flashes at aircraft and balloon altitudes depends on initial parameters. *Journal of Geophysical Research: Space Physics*, *118*(5), 2333–2339. https://doi.org/10.1002/jgra.50143

Heumesser, M., Chanrion, O., Neubert, T., Christian, H. J., Dimitriadou, K., Gordillo-Vazquez, F. J., et al. (2021). Spectral observations of optical emissions associated with terrestrial gamma-ray flashes. *Geophysical Research Letters*, *48*(4), 2020GL090700. https://doi.org/10.1029/2020GL090700

Inan, U. S., Cohen, M. B., Said, R. K., Smith, D. M., & Lopez, L. I. (2006). Terrestrial gamma ray flashes and lightning discharges. *Geophysical Research Letters*, *33*(18), L18802. https://doi.org/10.1029/2006GL027085

Janowiak, J., Joyce, B., & Xie, P. (2017). In A. Savtchenko (Ed.), *NCEP/CPC L3 Half Hourly 4 km Global (60°S–60°N) Merged IR V1* [Dataset]. Goddard Earth Sciences Data and Information Services Center (GES DISC). https://doi.org/10.5067/P4HZB9N27EKU

Lü, F., Zhu, B. Y., Zhou, H. L., Rakov, V. A., Xu, W. W., & Qin, Z. L. (2013). Observations of compact intracloud lightning discharges in the northernmost region (51°N) of China. *Journal of Geophysical Research-Atmospheres*, *118*(10), 4458–4465. https://doi.org/10.1002/jgrd.50295

Lu, G., Blakeslee, R. J., Li, J., Smith, D. M., Shao, X. M., McCaul, E. W., et al. (2010). Lightning mapping observation of a terrestrial gamma-ray flash. *Geophysical Research Letters*, *37*(11), L11806. https://doi.org/10.1029/2010GL043494

Lyu, F. (2024). Data for "Source altitude of energetic in-cloud pulses inside thunderstorms and implication for the intrinsic brightness of terrestrial gamma-ray flashes" [Dataset]. *Zenodo*. https://doi.org/10.5281/zenodo.13284686

Lyu, F., & Cummer, S. A. (2018). Energetic radio emissions and possible terrestrial gamma-ray flashes associated with downward propagating negative leaders. *Geophysical Research Letters*, *45*(19), 10764–10771. https://doi.org/10.1029/2018GL079424

Lyu, F., Cummer, S. A., Briggs, M., Marisaldi, M., Blakeslee, R. J., Bruning, E., et al. (2016). Ground detection of terrestrial gamma ray flashes from distant radio signals. *Geophysical Research Letters*, *43*(16), 8728–8734. https://doi.org/10.1002/20162GL070154

Lyu, F., Cummer, S. A., Briggs, M. S., Smith, D. M., Mailyan, B., & Lesage, S. (2021). Terrestrial gamma-ray flashes can be detected with radio measurements of energetic in-cloud pulses during thunderstorms. *Geophysical Research Letters*, *48*(11), e2021GL093627. https://doi.org/10.1029/2021GL093627

Lyu, F., Cummer, S. A., Krehbiel, P. R., Rison, W., Briggs, M. S., Crame, E., et al. (2018). Very high frequency radio emissions associated with the production of terrestrial gamma-ray flashes. *Geophysical Research Letters*, *45*(4), 2097–2105. https://doi.org/10.1002/2018GL077102

Lyu, F., Cummer, S. A., & McTague, L. (2015). Insights into high peak current in-cloud lightning events during thunderstorms. *Geophysical Research Letters*, *42*(16), 6836–6843. https://doi.org/10.1002/2015GL065047

Mailyan, B. G., Xu, W., Celestin, S., Briggs, M. S., Dwyer, J. R., Cramer, E. S., et al. (2019). Analysis of individual terrestrial gamma-ray flashes with lightning leader models and fermi gamma-ray burst monitor data. *Journal of Geophysical Research: Space Physics*, *124*(8), 7170–7183. https://doi.org/10.1029/2019JA026912

Marisaldi, M., Fuschino, F., Labanti, C., Galli, M., Longo, F., Del Monte, E., et al. (2010). Detection of terrestrial gamma ray flashes up to 40 MeV by the AGILE satellite. *Journal of Geophysical Research*, *115*(A3), A00E13. https://doi.org/10.1029/2009JA014502

Naud, C. M., Muller, J. P., Clothiaux, E. E., Baum, B. A., & Menzel, W. P. (2005). Intercomparison of multiple years of MODIS, MISR and radar cloud-top heights. *Annales Geophysicae*, *23*(7), 2415–2424. https://doi.org/10.5194/angeo-23-2415-2005

Østgaard, N., Neubert, T., Reglero, V., Ullaland, K., Yang, S., Genov, G., et al. (2019). First 10 months of TGF observations by ASIM. *Journal of Geophysical Research: Atmospheres*, *124*(24), 14024–14036. https://doi.org/10.1029/2019JD031214

Pu, Y., Cummer, S. A., Lyu, F., Briggs, M., Mailyan, B., Stanbro, M., & Roberts, O. (2019). Low frequency radio pulses produced by terrestrial gamma-ray flashes. *Geophysical Research Letters*, *46*(12), 6990–6997. https://doi.org/10.1029/2019GL082743

Qin, Z., Chen, M., Zhu, B., & Du, Y. P. (2017). An improved ray theory and transfer matrix method-based model for lightning electromagnetic pulses propagating in Earth-ionosphere waveguide and its applications. *Journal of Geophysical Research: Atmospheres*, *122*(2), 712–727. https://doi.org/10.1002/2016JD025599

Qin, Z., Cummer, S. A., Chen, M., Lyu, F., & Du, Y. (2019). A comparative study of the ray theory model with the finite difference time domain model for lightning sferic transmission in Earth-ionosphere waveguide. *Journal of Geophysical Research-Atmospheres*, *124*(6), 3335–3349. https://doi.org/10.1029/2018JD029440

Roberts, O. J., Fitzpatrick, G., Stanbro, M., McBreen, S., Briggs, M. S., Holzworth, R. H., et al. (2018). The First Fermi-GBM Terrestrial Gamma Ray Flash Catalog. *Journal of Geophysical Research: Space Physics*, *123*(5), 4381–4401. https://doi.org/10.1029/2017JA024837

Shao, X. M., Hamlin, T., & Smith, D. M. (2010). A closer examination of terrestrial gamma-ray flash-related lightning processes. *Journal of Geophysical Research*, *115*(A6), A00E30. https://doi.org/10.1029/2009JA014835

Shao, X. M., Lay, E. H., & Jacobson, A. R. (2013). Reduction of electron density in the night-time lower ionosphere in response to a thunderstorm. *Nature Geoscience*, *6*(1), 29–33. https://doi.org/10.1038/ngeo1668

Smith, D. A., Heavner, M. J., Jacobson, A. R., Shao, X. M., Massey, R. S., Sheldon, R. J., & Wiens, K. C. (2004). A method for determining intracloud lightning and ionospheric heights from VLF/LF electric field records. *Radio Science*, *39*(1), RS1010. https://doi.org/10.1029/2002rs002790

Smith, D. A., Shao, X. M., Holden, D. N., Rhodes, C. T., Brook, M., Krehbiel, P. R., et al. (1999). A distinct class of isolated intracloud lightning discharges and their associated radio emissions. *Journal of Geophysical Research*, *104*(D4), 4189–4212. https://doi.org/10.1029/1998JD200045

Smith, D. M., Hazelton, B. J., Grefenstette, B. W., Dwyer, J. R., Holzworth, R. H., & Lay, E. H. (2010). Terrestrial gamma ray flashes correlated to storm phase and tropopause height. *Journal of Geophysical Research*, *115*(A8), A00E49. https://doi.org/10.1029/2009JA014853

Smith, D. M., Lopez, L. I., Lin, R. P., & Barrington-Leigh, C. P. (2005). Terrestrial gamma-ray flashes observed up to 20 MeV. *Science*, *307*(5712), 1085–1088. https://doi.org/10.1126/science.1107466

Stanley, M. A., Shao, X. M., Smith, D. M., Lopez, L. I., Pongratz, M. B., Harlin, J. D., et al. (2006). A link between terrestrial gamma-ray flashes and intracloud lightning discharges. *Geophysical Research Letters*, *33*(6), L06803. https://doi.org/10.1029/2005GL025537

Tilles, J. N., Krehbiel, P. R., Stanley, M. A., Rison, W., Liu, N., Lyu, F., et al. (2020). Radio interferometer observations of an energetic in-cloud pulse reveal large currents generated by relativistic discharges. *Journal of Geophysical Research: Atmospheres*, *125*(20), e2020JD032603. https://doi.org/10.1029/2020JD032603

Ursi, A., Marisaldi, M., Dietrich, S., Tavani, M., Tiberia, A., & Porcù, F. (2019). Analysis of thunderstorms producing terrestrial gamma ray flashes with the Meteosat second generation. *Journal of Geophysical Research: Atmospheres*, *124*(23), 12667–12682. https://doi.org/10.1029/2018jd030149

Wait, J. R., & Spies, K. P. (1964). *Characteristics of the Earth-ionosphere waveguide for VLF radio waves*. National Institute of Standards and Technology. https://doi.org/10.6028/NBS.TN.300

Wu, T., Dong, W., Zhang, Y., Funaki, T., Yoshida, S., Morimoto, T., et al. (2012). Discharge height of lightning narrow bipolar events. *Journal of Geophysical Research*, *117*(D5), D05119. https://doi.org/10.1029/2011JD017054

Xu, W., Celestin, S., & Pasko, V. P. (2012). Source altitudes of terrestrial gamma-ray flashes produced by lightning leaders. *Geophysical Research Letters*, *39*(8), L08801. https://doi.org/10.1029/2012GL051351

Xu, W., Celestin, S., & Pasko, V. P. (2015). Optical emissions associated with terrestrial gamma ray flashes. *Journal of Geophysical Research-Space Physics*, *120*(2), 1355–1370. https://doi.org/10.1002/2014JA020425

Zhang, H., Lu, G., Lyu, F., Ahmad, M. R., Qie, X., Cummer, S. A., et al. (2020). First measurements of low-frequency sferics associated with terrestrial gamma-ray flashes produced by equatorial thunderstorms. *Geophysical Research Letters*, *47*(17), e2020GL089005. https://doi.org/10.1029/2020gl089005

Zhang, H., Lu, G., Qie, X., Jiang, R., Fan, Y., Tian, Y., et al. (2016). Locating narrow bipolar events with single-station measurement of low-frequency magnetic fields. *Journal of Atmospheric and Solar-Terrestrial Physics*, *143*, 88–101. https://doi.org/10.1016/j.jastp.2016.03.009